2025 International Conference on Quantum Communications, Networking, and Computing (QCNC) | 979-8-3315-3159-1/25/$31.00 ©2025 IEEE | DOI: 10.1109/QCNC64685.2025.00090

Towards Motion Sensing Using Asymmetric Coupled Quantum Dots

Kyle Wright
Department of Applied Mathematics
University of California, Merced
Merced, CA, U.S.
kwright11@ucmerced.edu

Roummel Marcia
Department of Applied Mathematics
University of California, Merced
Merced, CA, U.S.
rmarcia@ucmerced.edu

Michael Scheibner
Department of Physics
University of California, Merced
Merced, CA, U.S.
mscheibner@ucmerced.edu

Boaz Ilan
Department of Applied Mathematics
University of California, Merced
Merced, CA, U.S.
bilan@ucmerced.edu

***Abstract*—Quantum sensing and metrology are one of the most broad and advanced areas of quantum information and technology. We investigate the possibility of using coupled quantum dots for motion detection. The system consists of two coupled vertically-stacked asymmetric quantum dots in the presence of a tunable electric field. By measuring the system's excited energy levels at varying electric fields, the distance between the dots can be extracted from photoluminescence spectral patterns. This is modeled by an inverse eigenvalue difference problem associated with the quantum Hamiltonian. We develop algebraic and computational methods along with a warm-starting strategy to solve this problem. Examples demonstrate the accuracy and sensing resolution of this approach.**

***Index Terms*—quantum sensing; inverse eigenvalue problems, optimization**

I. Introduction

Quantum sensing and metrology has become a broad field as well as an emergent technology that promises to provide unprecedented precision measurement and sensing capabilities [1]–[4]. Quantum sensors utilize quantum phenomena, such as superposition, coherence, tunneling, and entanglement, to measure a physical quantity beyond what can be done using classical sensors. This promises to achieve high-resolution sensing of gravitation, acoustic waves, and electromagnetic fields with a wide range of applications [3]–[14].

In this paper, we explore the idea of quantum sensing of motion using semiconductor quantum dots in the presence of a tunable electric field. We consider a system of two coupled quantum dots, which are embedded in a dynamic environment, such as a crystal lattice subject to strain, or pairs of colloidal quantum dots formed on DNA origami templates [15]–[18]. Given measurements of the system's energy levels as an external electric field is varied, we extract the system's intrinsic features and recover the distance between the quantum dots. This paradigm can be used to detect motion, strain, and structural deformation. In particular, this has applications to bioimaging [19], signal processing circuitry [20], and quantum cellular automata for circuits [21] Our approach is to model the system using an effective quantum Hamiltonian and use an efficient computational technique to "read out" the Hamiltonian from photoluminescence (PL) measurements. This allows to infer the interdot distance. Examples using parameters for self-assembled InAs/GaAs quantum dots demonstrate that this approach is sensitive enough to measure accurately distances of a few nanometers. The prospect to generalize this approach and its potential applications are discussed.

This research is partially supported by NSF grants DMS 1840265 and DMS 2125510.

II. Background

When two quantum dots are near each other they form a coupled quantum dot (CQD) pair. CQDs have long radiative lifetimes and enable *in situ* control of exchange interactions, coherent phonon effects, and other useful features [15]. In particular, they give rise to spatially extended states due to the interdot tunnel coupling of electrons, holes and / or excitons.

When an electric field is applied to vertically-stacked asymmetric pairs of quantum dots (such as InGaAs/InAs), the PL spectral patterns exhibit crossings and anticrossings [22], [23]. These spectra are sensitive to changes in the intradot distance [24]. Any change of distance between the dots serves as a proxy for their relative motion due to mechanical strain or forces that move them within their environment. Our idea is to leverage this sensitivity by measuring the PL spectra as an external electric field is varied and use this data to recover the distance between the dots. In this way, the proposed approach can be used to detect and characterize motion.

III. Formulation

In this section, we formulate a general approach to recover the distance between two quantum dots in a CQD given measurements of their PL spectra for a few values of an applied electric field. This approach entails a numerical algorithm, which is based on modeling the discrete energy levels of a CQD as eigenvalues of an effective quantum Hamiltonian [23],

979-8-3315-3159-1/25/$31.00 ©2025 IEEE
DOI 10.1109/QCNC64685.2025.00090

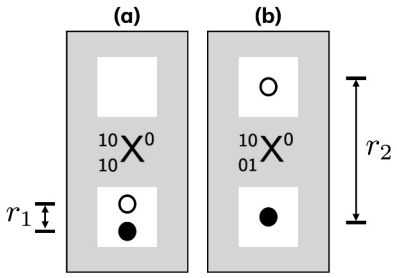

Fig. 1: A coupled quantum dot (CQD) system composed of two quantum dots (white boxes) contains an exciton (electron-hole pair) with two possible states. (a) For an intradot exciton, denoted by $^{10}_{10}\mathsf{X}^0$, both the electron (●) and hole (○) occupy the same dot. (b) For an interdot exciton, denoted by $^{10}_{01}\mathsf{X}^0$, the electron and hole occupy different dots. The distances between the electron and hole in the intradot and interdot states are r_1 and r_2, respectively.

[25]. The Hamiltonian's entries are extracted from the PL measurements using an inverse eigenvalue method [26]. The distance between the dots is recovered from one of the Hamiltonian terms. As an aside, the electric dipole moments, polarizabilities and hole tunneling strength of the dots are recovered as well, which could prove useful for extending this approach.

We propose using an asymmetric CQD pair, containing a neutral exciton. This setup has been shown to create electron and hole resonances that occur at different electric field values. This allows for a setup where one dot has a smaller direct transition energy, with the electron being localized in one dot when the hole levels are brought into resonance. This results in two possible charge states. As shown in Fig. 1, the interdot charge state occurs when the electron and hole reside in different dots, while the intradot charge state occurs when the electron and hole reside within the same dot.

The notation $^{e_B e_T}_{h_B h_T}\mathsf{X}^{\mathsf{Q}}$ represents a specific CQD state, where e_B and e_T correspond to the number of electrons in the bottom and top dots, respectively. Similarly, the number of holes in the bottom and top dots is denoted by h_B and h_T, respectively. The superscript Q is the net charge, which is zero for a neutral exciton.

The steady-state energy levels of the CQD correspond to eigenvalues of the quantum Hamiltonian. Our CQD system is described by a 2×2 symmetric matrix of the form

$$H(F) = \begin{bmatrix} E_1(F) & t \\ t & E_2(F) \end{bmatrix}. \tag{1}$$

The diagonal elements of H describe quadratic deviations from the ground state energy line. These elements are given by

$$E_i(F) = E_i(0) - p_i F + \beta_i F^2, \quad i = 1, 2\ , \tag{2}$$

which depends on the electric field strength F via a quadratic Stark shift (see [27]). The constants $E_1(0)$ and $E_2(0)$ are

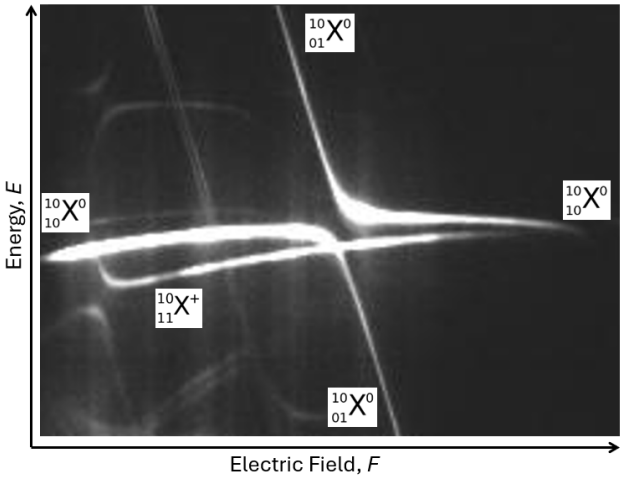

Fig. 2: Electric field dispersed photoluminescence (PL) spectrum of a CQD pair. The intradot neutral exciton transition, $^{10}_{10}\mathsf{X}^0$, and the interdot neutral exciton, $^{10}_{01}\mathsf{X}^0$, are two prominent transitions. The intradot transition from a positive trion, $^{10}_{11}\mathsf{X}^+$, is also prominent, but not discussed in this work.

the eigenenergies absent the presence of an electric field. The coefficient t is the hole tunneling strength. The quadratic term coefficient β_i corresponds to the polarizability of the ground-state electron and hole wave functions. The coefficients of the linear term are the electric dipole moments p_i, given by

$$p_i = e r_i\ , \tag{3}$$

where e is electron charge and r_i is the distance between the electron and hole. Specifically, r_2 is the interdot distance. Due to the location of the electron and hole within separate quantum dots, r_2 well-approximates the distance between the dots. Hence, we seek to recover r_2.

Figure 2 shows experimental data of electric field dependent PL spectra of a CQD pair, which exhibits the intradot and interdot neutral exciton transitions. Figure 3 shows simulated data analogous to Fig. 2. For this simulation, the diagonal entries in the Hamiltonian, $E_1(F)$ and $E_2(F)$, are defined by Eq. (2) with electric dipole moments $p_1 = 0.0004, p_2 = -1$ [10^{-6} e·cm], polarizabilities $\beta_1 = 0.0007, \beta_2 = 0.0005$ [C·cm^2/kV], and hole tunneling strength $t = 0.3$ meV. The transition between charge states occurs at approximately $F^* \approx 13.5$ kV/cm, where $E_1(F^*) = E_2(F^*)$. This figure depicts two key features: (1) as the applied electric field F varies, the energies $\xi_1(F)$ and $\xi_2(F)$ transition between the two CQD states, $^{10}_{10}\mathsf{X}^0$ and $^{10}_{01}\mathsf{X}^0$; and (2) the asymptotic relationships $\xi_1(F)$ and $\xi_2(F)$ and the deviations from the ground state energy levels, which are the $E_1(F)$ and $E_2(F)$ above. Our approach for recovering r_2 is described in the next section.

IV. Numerical Approach

We seek to recover r_2 given the energies for a set of electric field values. Recall that r_2 is obtained from p_2 (see (3)). We

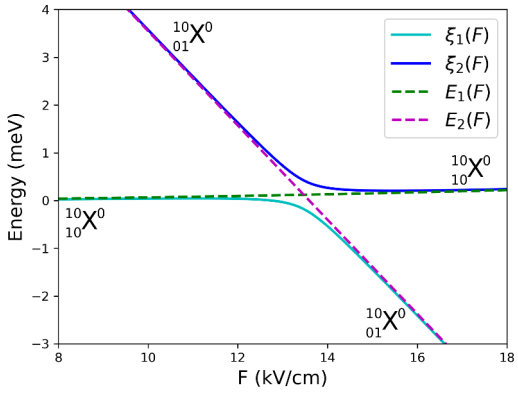

Fig. 3: Simulated energy levels of the CQD's quantum Hamiltonian as the applied electric field is varied. These spectra exhibit asymptotic relationships between the eigenenergies, $\xi_1(F)$ and $\xi_2(F)$, and the diagonal entries, $E_1(F)$ and $E_2(F)$. For $F < F^*$, $\xi_1(F) \to E_1(F)$ and $\xi_2(F) \to E_2(F)$ as F decreases; and in contrast, for $F > F^*$, $\xi_1(F) \to E_2(F)$ and $\xi_2(F) \to E_1(F)$ as F increases.

do so by recovering all the coefficients of $H(F)$ in (1). Specifically, we formulate our problem as follows: Given the measurements of the energies $\{\xi_1(F_k), \xi_2(F_k)\}_{k=1}^K$ for a small set of applied electric field values $F_k, k = 1, 2, \ldots, K$, we seek to recover the coefficients $\{t, E_1(0), p_1, \beta_1, E_2(0), p_2, \beta_2\}$. This problem can be formulated as an inverse eigenvalue problem (IEP) (see [28], [29]), which can be solved by considering the eigenvalues of $H(F)$.

Note that the eigenvalues of $H(F_k)$ are the roots of its characteristic polynomial, *i.e.*,

$$\det\big(H(F_k) - \xi I_2\big) = 0 \tag{4}$$

for $\xi \in \{\xi_1, \xi_2\}$, where we suppress the dependence of ξ_1 and ξ_2 (and of ξ, in general) on F_k for notational convenience. Here I_2 is the 2×2 identity matrix. More explicitly, (4) can be written as

$$E_1(F_k)E_2(F_k) - (E_1(F_k) + E_2(F_k))\xi + \xi^2 - t^2 = 0. \tag{5}$$

In addition, since the eigenvalues are roots of the characteristic polynomial, the characteristic polynomial of $H(F_k)$ is also given by

$$\begin{aligned} \det\big(H(F_k) - \xi\big) &= (\xi_1 - \xi)(\xi_2 - \xi) && \text{(6a)} \\ &= \xi_1\xi_2 - (\xi_1 + \xi_2)\xi + \xi^2. && \text{(6b)} \end{aligned}$$

Comparing the coefficients in (5) with those in (6b), we see that

$$\begin{aligned} E_1(F_k)E_2(F_k) - t^2 &= \xi_1\xi_2 && \text{(7a)} \\ E_1(F_k) + E_2(F_k) &= \xi_1 + \xi_2 && \text{(7b)} \end{aligned}$$

From (7b), we see that $E_2(F_k) = \xi_1 + \xi_2 - E_1(F_k)$. Substituting this expression for $E_2(F_k)$ in (7a), we can define functions whose roots are the desired coefficients. In particular, the functions are given by

$$\begin{aligned} \mathscr{F}_1(t, c_1; F_k) &= E_1(F_k)^2 - E_1(F_k)(\xi_1 + \xi_2) + \xi_1\xi_2 + t^2, && \text{(8a)} \\ \mathscr{F}_2(c_2; c_1, F_k) &= E_1(F_k) + E_2(F_k) - \xi_1 - \xi_2, && \text{(8b)} \end{aligned}$$

where we denote the coefficients in $E_1(F)$ and $E_2(F)$ by $c_1 = (E_1(0), p_1, \beta_1)$ and $c_2 = (E_2(0), p_2, \beta_2)$, respectively.

We recover the coefficients sequentially, meaning we first find the roots of $\mathscr{F}_1$. Having obtained t and c_1, we use these to solve for c_2 by finding the roots of $\mathscr{F}_2$. In other words, $E_1(F_k)$ in (8b) is simply a scalar that can be computed using c_1 from (8a) and F_k, and consequently, the remaining dependence of $\mathscr{F}_2$ is only on c_2. This approach is similarly found in [26].

To find the root of $\mathscr{F}_1$ in (8a), we solve the following problem, whose minima correspond to the root of the $\mathscr{F}_1$:

$$\underset{t, c_1}{\text{minimize}} \quad \mathcal{L}_{\mathcal{F}}(t, c_1) = \sum_{k=1}^{K} \big[\mathscr{F}_1(t, c_1; F_k)\big]^2, \tag{9}$$

where $\mathcal{F} = \{F_1, F_2, \ldots, F_K\}$. In the absence of measurement errors, any four values of F, *i.e.*, $K = 4$, are both necessary and sufficient for solving (9) to obtain t, $E_1(0)$, p_1, and β_1. Those same values of F can then be used to solve a similar minimization problem for $E_2(0)$, p_2, and β_2 using (8b). In our code, we use the *trust-exact* method in Python's *scipy.optimize.minimize* package.

Optimization methods for IEPs of this form require good initial iterates to converge to a solution [30]. An existing approach to recover r_2 works as follows. When the electric field is far from the transition between charge states (see Fig. 2), ξ_1 and ξ_2 well approximate E_1 and E_2. Taking measurements at several F values sufficiently far from the transition between charge states, one can recover the coefficients in $E_1(F)$ and $E_2(F)$, from which r_2 is readily obtained. We refer to this as the asymptotic approach. We use a similar concept for initializing our optimization.

Given $K \geq 4$ values of F, we first find the three that have the greatest difference eigenvalue difference, $|\xi_2 - \xi_1|$ for use in computing initial values for $E_1(0)$, $E_2(0)$, p_1, p_2, β_1, and β_2. The initial values are computed using least squares. The initial value of t can then be computed from (8a) using the previously determined initial values. See [26] for further details.

V. Numerical Experiments

We conducted numerical experiments to test the efficacy of the proposed approach outlined in Sec. IV using noisy measurements. For the results shown, we used simulated measurement values from Fig. 3. These values were created with $c_1 = (0, 0.0004, 0.0007)$, $c_2 = (13.5, -1, 0.0005)$, and $t = 0.3$.

Note that (9) is dependent upon the values $F_1, \ldots, F_K$ chosen. As F becomes more distant from the intersection of $E_1(F)$ and $E_2(F)$, $E_1(F) \to \xi_1(F)$ or $E_1(F) \to \xi_2(F)$ and it becomes more difficult to recover t numerically from (8a). This results in more iterations for the optimization function to reach the same value (see Fig. 4) and is exacerbated by

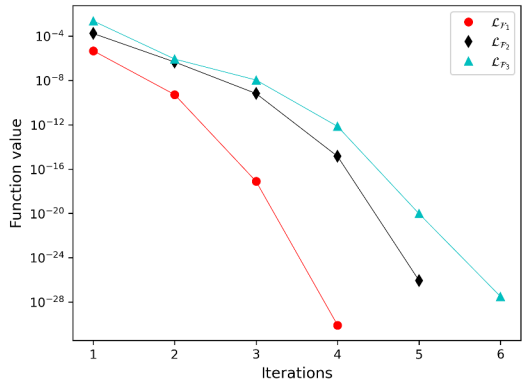

Fig. 4: Objective function values as functions of iterations. Each $\mathcal{L}_{\mathcal{F}_i}$ for $i = 1, 2, 3$ (as defined in (9)) corresponds to different sets of values of F, with $\mathcal{F}_1 = \{10, 12, 14, 16\}$, $\mathcal{F}_2 = \{6, 8, 18, 20\}$, and $\mathcal{F}_3 = \{2, 4, 22, 24\}$. Note that as the values of F become more distant from the intersection of $E_1(F)$ and $E_2(F)$ (near $F = 13.5$), the more iterations are required for the optimization approach to converge.

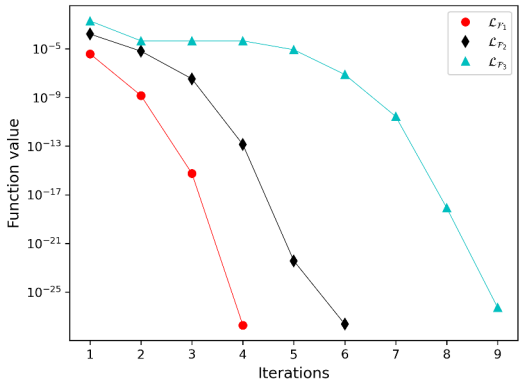

Fig. 5: Objective function values $\mathcal{L}_{\mathcal{F}_i}$ as functions of iterations, with 0.02 perturbations applied to $\xi_1(F_k)$ and $\xi_2(F_k)$. The functions $\mathcal{L}_{\mathcal{F}_1}$, $\mathcal{L}_{\mathcal{F}_2}$, and $\mathcal{L}_{\mathcal{F}_3}$ are as in Fig. 4.

perturbations to $\xi_1(F)$ and $\xi_2(F)$ (see Fig. 5). Additionally, this effect becomes more pronounced as K increases. By also including values of F near the intersection of $E_1(F)$ and $E_2(F)$, the relative contribution of t to (8a) becomes more pronounced and t becomes easier to recover.

Measurement noise is expected in the energies. To measure the impact of noise on the proposed approach, we introduce perturbations at each $\xi_i(F_k)$, for $F \in [10, 12, 14, 16]$, as

$$\tilde{\xi}_i(F_k) = \xi_i(F_k) + \tau_i(F_k)\varepsilon, \tag{10}$$

where $\tau_i(F_k) \in \{-1, 1\}$ is a binary random variable and $0 < \varepsilon \ll 1$ is the error size. To determine the effects of noise on our proposed approach, we simulated noisy measurements using (10) for different values of ε. We implemented our method using these noisy measurements and observed the relative error in the coefficient $\hat{r}_2$, as shown in Fig. 6. This figure demonstrates an $O(\varepsilon)$ relative error in the recovered r_2. We also observed an $O(\varepsilon)$ relative error for the other coefficients in the Hamiltonian. This shows that the proposed method is both robust in the presence of noise and produces a predictable increase in the accuracy as noise is reduced.

We also seek to compare our proposed approach to the asymptotic approach. Using our approach, the relative error in the recovered r_2 decreases with ε down to machine precision, while using measurements for only 4 values of F (see Fig. 6). In contrast, the traditional approach, given some set of values of F, contains additional modelling error. This error dependent upon how well ξ_1 and ξ_2 approximate E_1 and E_2. For example, when applying the asymptotic approach to simulated eigenenergy data for $F \in [9.5, 10] \cup [16, 16.5]$, the relative error of r_2 does not go below 10^{-2}, as seen in Fig. 3. Despite the values of F used, the modelling error results in a lower bound in error of r_2, even if there is no

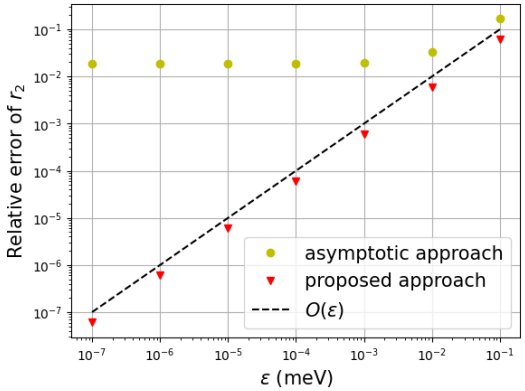

Fig. 6: Relative error ($|r_2 - \hat{r}_2|/|r_2|$) in recovering the interdot distance $\hat{r}_2$ as the measurement error ε varies. Using the traditional ("asymptotic") method, the relative error does not decrease below 10^{-2}. Using our approach, the relative error scales as $O(\varepsilon)$ down to machine precision. We observe similar results for all other coefficients in the Hamiltonian $H(F)$.

measurement error and/or measurements for many values of F when applying the asymptotic method.

To put measurement error into context, it depends on the linewidth of the PL spectra, which, in turn, depends on the resolution of the system as well as the fluctuations felt by the state/transition due to charges. For intradot transitions the linewidth is limited by instrument resolution ($0.01 - 0.5$meV depending on the spectrometer) or with highest resolution by the lifetime ($\approx$ 0.001-0.02 meV). For interdot transitions the electronic fluctuations and dot separation determine the linewidth (typically 0.08meV-0.5meV). These instrument resolutions provide an upper bound for expected noise values.

VI. Discussion

Our proposed quantum sensor could recover the distance between CQDs with high accuracy. This sensor would be

robust in the presence of noise, including environmental and measurement noise, and achieve the same or higher accuracy than existing methods while requiring significantly fewer measurements. Moreover, our method simultaneously recovers other physical parameters, including the tunneling rate and polarizabilities. This study is the starting point for a quantum approach to motion sensing. In contrast to the recombination lifetime-limited exciton, one could also consider charge and spin states that are long lived, such the ground states of a positive trion. Our approach can also be generalized to include quantum coherence and interference measurements, which would enable even greater sensitivity to motion.

Such quantum sensors can be applied to differentiate between changes in eigenenergies due to strain *vs.* CQD separation due to mechanical or electromagnetic forces. In the case of strain, dot separation changes minimally, with greater changes to the barrier height and/or the dot confinement potential. Hence, there are observable changes in the tunnel coupling and the energies of the states, but not their response to the electric field (the dipole moments).

Another CQD system can be realized using colloidal quantum dots that are assembled via DNA origami templates. Here, the dot separation can change, impacting both the tunnel coupling and dipole moments, but not the electron and hole's eigenenergies. Such sensors could be employed as anti-tempering markers, or for structural health monitoring by early detection of material fatigue and nano-/micro-fissures.

For future work we will consider more complex systems involving more quantum dots. Consequently, this could require more sophisticated modeling and optimization approaches.

REFERENCES

[1] E. O. Göbel and U. Siegner, *Quantum Metrology: Foundation of Units and Measurements*. John Wiley & Sons, 2015.

[2] C. L. Degen, F. Reinhard, and P. Cappellaro, "Quantum sensing," *Reviews of modern physics*, vol. 89, no. 3, p. 035002, 2017.

[3] S. Pirandola, B. R. Bardhan, T. Gehring, C. Weedbrook, and S. Lloyd, "Advances in photonic quantum sensing," *Nature Photonics*, vol. 12, no. 12, pp. 724–733, 2018.

[4] Y. L. Len, T. Gefen, A. Retzker, and J. Kołodyński, "Quantum metrology with imperfect measurements," *Nature Communications*, vol. 13, no. 1, p. 6971, 2022.

[5] S. Walborn, A. Pimentel, L. Davidovich, and R. de Matos Filho, "Quantum-enhanced sensing from hyperentanglement," *Physical Review A*, vol. 97, no. 1, p. 010301, 2018.

[6] B. Stray, A. Lamb, A. Kaushik, J. Vovrosh, A. Rodgers, J. Winch, F. Hayati, D. Boddice, A. Stabrawa, A. Niggebaum *et al.*, "Quantum sensing for gravity cartography," *Nature*, vol. 602, no. 7898, pp. 590–594, 2022.

[7] K. J. Satzinger, Y. Zhong, H.-S. Chang, G. A. Peairs, A. Bienfait, M.-H. Chou, A. Cleland, C. R. Conner, É. Dumur, J. Grebel *et al.*, "Quantum control of surface acoustic-wave phonons," *Nature*, vol. 563, no. 7733, pp. 661–665, 2018.

[8] C.-Y. Lai, M. Di Ventra, M. Scheibner, and C.-C. Chien, "Tunable current circulation in triangular quantum-dot metastructures," *Europhysics Letters*, vol. 123, no. 4, p. 47002, 2018.

[9] P. Dugar, M. Scheibner, and C.-C. Chien, "Geometry-based circulation of local photonic transport in a triangular metastructure," *Physical Review A*, vol. 102, no. 2, p. 023704, 2020.

[10] C. Jennings, X. Ma, T. Wickramasinghe, M. Doty, M. Scheibner, E. Stinaff, and M. Ware, "Self-assembled inas/gaas coupled quantum dots for photonic quantum technologies," *Advanced Quantum Technologies*, vol. 3, no. 2, p. 1900085, 2020.

[11] M. Scheibner, A. S. Bracker, D. Kim, and D. Gammon, "Essential concepts in the optical properties of quantum dot molecules," *Solid State Communications*, vol. 149, no. 35-36, pp. 1427–1435, 2009.

[12] A. Vamivakas, Y. Zhao, S. Fält, A. Badolato, J. Taylor, and M. Atatüre, "Nanoscale optical electrometer," *Physical Review Letters*, vol. 107, no. 16, p. 166802, 2011.

[13] S. Ramanathan, G. Petersen, K. Wijesundara, R. Thota, E. A. Stinaff, M. L. Kerfoot, M. Scheibner, A. S. Bracker, and D. Gammon, "Quantum-confined stark effects in coupled inas/gaas quantum dots," *Applied Physics Letters*, vol. 102, no. 21, 2013.

[14] J. Anders, T. Pfau, J. Wrachtrup, M. B. Plenio, F. Jelezko, and K. Lips, "Towards ic-based quantum sensing-recent achievements and future research trends," in *2018 48th European Solid-State Device Research Conference (ESSDERC)*. IEEE, 2018, pp. 122–125.

[15] C. Jennings, X. Ma, T. Wickramasinghe, M. Doty, M. Scheibner, E. Stinaff, and M. Ware, "Self-assembled inas/gaas coupled quantum dots for photonic quantum technologies," *Advanced Quantum Technologies*, vol. 3, no. 2, p. 1900085, 2020.

[16] S. G. Carter, A. S. Bracker, M. K. Yakes, M. K. Zalalutdinov, M. Kim, C. S. Kim, B. Lee, and D. Gammon, "Tunable coupling of a double quantum dot spin system to a mechanical resonator," *Nano Letters*, vol. 19, no. 9, pp. 6166–6172, 2019.

[17] P. Rahmani, M. Goodlad, Y. Zhang, Y. Li, and T. Ye, "One-step ligand-exchange method to produce quantum dot–dna conjugates for dna-directed self-assembly," *ACS Applied Materials & Interfaces*, vol. 14, no. 42, pp. 47 359–47 368, 2022.

[18] Z. Deng, A. Samanta, J. Nangreave, H. Yan, and Y. Liu, "Robust dna-functionalized core/shell quantum dots with fluorescent emission spanning from uv–vis to near-ir and compatible with dna-directed self-assembly," *Journal of the American Chemical Society*, vol. 134, no. 42, pp. 17 424–17 427, 2012.

[19] M. Jonas, Y. Yao, P. T. C. So, and C. F. Dewey, "Detecting single quantum dot motion with nanometer resolution for applications in cell biology," *IEEE Transactions on NanoBioscience*, vol. 5, no. 4, pp. 246–250, 2006.

[20] W. H. Lee and P. Mazumder, "Motion detection by quantum-dots-based velocity-tuned filter," *IEEE Transactions on Nanotechnology*, vol. 7, no. 3, pp. 355–362, 2008.

[21] J.-C. Jeon and C. Seo, "Quantum-dot cellular automata demultiplexer with minimum design costs with energy dissipation analysis and physical proof for reliable nano-communication systems," *Heliyon*, vol. 10, no. 16, 2024.

[22] E. A. Stinaff, M. Scheibner, A. S. Bracker, I. V. Ponomarev, V. L. Korenev, M. E. Ware, M. F. Doty, T. L. Reinecke, and D. Gammon, "Optical signatures of coupled quantum dots," *Science*, vol. 311, no. 5761, pp. 636–639, 2006.

[23] M. Scheibner, M. Doty, I. V. Ponomarev, A. S. Bracker, E. A. Stinaff, V. Korenev, T. Reinecke, and D. Gammon, "Spin fine structure of optically excited quantum dot molecules," *Physical Review B*, vol. 75, no. 24, p. 245318, 2007.

[24] M. Scheibner, A. S. Bracker, D. Kim, and D. Gammon, "Essential concepts in the optical properties of quantum dot molecules," *Solid state communications*, vol. 149, no. 35-36, pp. 1427–1435, 2009.

[25] I. V. Ponomarev, M. Scheibner, E. A. Stinaff, A. S. Bracker, M. Doty, S. Badescu, M. Ware, V. Korenev, T. Reinecke, and D. Gammon, "Theory of spin states in coupled quantum dots," *physica status solidi (b)*, vol. 243, no. 15, pp. 3869–3873, 2006.

[26] K. Wright, R. Marcia, M. Scheibner, and B. Ilan, "Parameterized inverse eigenvalue problem for quantum sensing," in *2023 IEEE 9th International Workshop on Computational Advances in Multi-Sensor Adaptive Processing (CAMSAP)*. IEEE, 2023, pp. 351–355.

[27] J. D. Mar, J. J. Baumberg, X. L. Xu, A. C. Irvine, and D. A. Williams, "Precise measurements of the dipole moment and polarizability of the neutral exciton and positive trion in a single quantum dot," *Phys. Rev. B*, vol. 95, p. 201304, May 2017.

[28] M. T. Chu, "Inverse eigenvalue problems," *SIAM Review*, vol. 40, no. 1, pp. 1–39, 1998.

[29] M. T. Chu and G. H. Golub, "Structured inverse eigenvalue problems," *Acta Numerica*, vol. 11, pp. 1–71, 2002.

[30] K. Wright, R. Marcia, and B. Ilan, "Numerical methods for a Schrödinger equation inverse eigenvalue problem," in *15th International Conference on Mathematical and Numerical Aspects of Wave Propagation*. Waves, 2022.